Inelastic distortional buckling of cantilevers

Dong-Sik Lee†

Department of Civil, Urban and Geosystem Engineering,
Seoul National University, Seoul 51-752, Korea

Mark Andrew Bradford‡

School of Civil and Environmental Engineering, The University of New South Wales,
UNSW Sydney, NSW 2052, Australia

Abstract.   Cantilevers are unique statically determinate structural elements with respect to their mode of overall buckling, in that the tension flange is the critical flange under gravity loading, and is the flange that deflects greatest during overall buckling. While this phenomenon does not complicate the calculation of the lateral buckling load, either theoretically or in structural design codes, it has been shown in previous research that the influence of distortion in the elastic buckling of cantilevers is not the same as that experienced in the elastic buckling of simply supported beams. This paper extends the study of the distortional buckling of cantilevers into the hitherto unconsidered inelastic range of structural response. A finite element method for studying the inelastic bifurcative instability of members whose cross-sections may distort during buckling is described, and the efficacy of the method is demonstrated. It is then used to study the inelastic distortional buckling of hot-rolled I-section cantilevers with two common patterns of residual stresses, and which may be restrained elastically from buckling by other structural elements.

Key words: buckling; cantilevers; distortional buckling; inelasticity; residual stresses; restraints.

1. Introduction

   Steel cantilevers are unique statically determinate structural members in regard to their mode of overall instability, since the tension flange is the flange that deflects most during buckling, in deference to the compression flange that deflects most during buckling in other structural members. When predicting the strength of a cantilever based on the limit state of lateral-torsional buckling, this phenomenon does not complicate the issue as the inelastic lateral-torsional buckling load, upon which the design rules given in national standards are based, is no more difficult to determine for a cantilever than that for a simply supported member. It has been shown that when the cross-section of a member has partial restraint (Bradford 1988, 1990, Ronagh *et al.* 2000), the assumptions upon which the lateral-torsional buckling strength is based (primarily the Vlasov assumption of an undeformable cross-section) are at best questionable. Moreover, when this assumption in Vlasov thin-walled theory is relaxed, elastic

---

†Post-doctoral Research Fellow
‡Professor

buckling studies have shown that determining the resulting lateral-distortional buckling load for a cantilever is not straightforward, either if the cantilever is unrestrained (Bradford 1992) or if it restrained partially (Bradford 1998, 1999) against buckling. This paper addresses the issue of the inelastic lateral-distortional buckling of cantilevers that are either unrestrained or elastically restrained against buckling.

Studies of the elastic lateral-torsional buckling of cantilevers have been widespread. Amongst these are the closed-form solution for the buckling of a doubly symmetric cantilever given in Trahair (1993), and for a monosymmetric cantilever reported by Wang and Kitipornchai (1986). Anderson and Trahair (1972), Attard (1984) and Attard and Bradford (1990) reported experimental and theoretical studies on unrestrained cantilevers, and Assadi and Roeder (1985) conducted theoretical and experimental studies of the buckling of continuously restrained cantilevers. These studies were restricted to elastic buckling, since inelastic buckling requires recourse to a consideration of yielding along the member, including monosymmetry induced in the cross-section due to the combined effects of in-plane bending and residual stresses, which is difficult to model. The first study of the inelastic lateral-torsional buckling of cantilevers appears to be that of Nethercot (1973), who used the finite element method. This theoretical technique was an approximation, since it modelled the yielding of the cantilever along its length as a stepped cantilever with a number of uniform elements, and this has been shown (Ronagh and Bradford 1994) to neglect some terms that may cause a convergence to an erroneous answer.

The finite element method has been the main tool for the analysis of the distortional buckling of cantilevers, and this has been restricted hitherto to the elastic range of structural response. There appear to be no studies of the inelastic lateral-distortional buckling of cantilevers reported in the open literature, and this aspect of applied stability theory is studied herein. A line element with 16 degrees of buckling freedom developed by the authors (Lee and Bradford 2002) is described briefly, and its application to the buckling of cantilevers is reported in this paper. The method allows for the inclusion of residual stresses induced in the hot-rolling process for universal beams, and for continuous elastic restraints against out-of-plane buckling. This finite element model is superior to existing software packages, in that it does not require the discretisation of the beam topology into a large number of shell-type elements, and because it is able to include residual stresses. Some pertinent results are given, and conclusions are drawn regarding the inelastic buckling of cantilevers.

2. Finite element method of buckling analysis

2.1. General

Lee and Bradford (2002) have reported a general finite element method of analysis for the inelastic lateral-distortional buckling of I-section members. For statically determinate members (in this case cantilever members), it requires an in-plane analysis to be undertaken, with a reference bending moment field M being subjected to a proportional loading regime under a load factor λ until uncoupled, out of plane buckling occurs at a critical load factor λ_{cr}. By treating the lengthwise buckling of the member as an assembly of line-type elements (whose lengthwise variation of buckling deformations are cubic polynomials), each of whose cross-sections may distort during buckling, it is possible to predict the buckling load by formulating an eigenproblem. Because of the influence of yielding, the cross-sections become monosymmetric under the combined effects of residual stresses and bending stresses, and since the member is subjected to a bending moment that generally varies along the length of the member, the yielding renders the
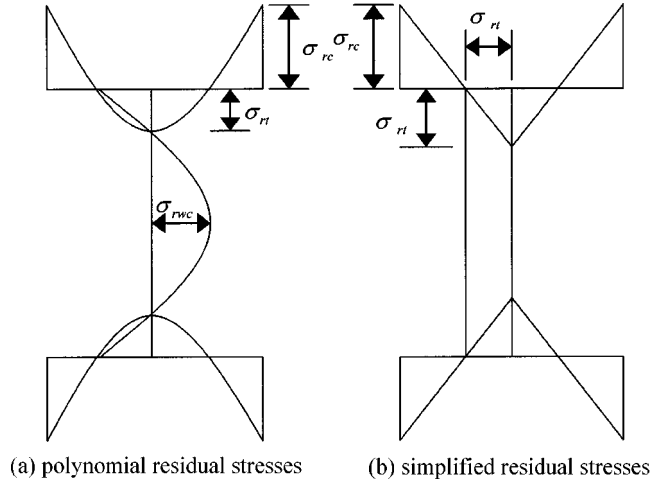
(a) polynomial residual stresses   (b) simplified residual stresses

Fig. 1 Residual stress pattern

member lengthwise as nonuniform.

2.2. In-plane analysis

A hot-rolled cross-section contains residual stresses f_r that are induced during cooling, and these can be thought of a residual strain field ε_r obtained by dividing the stress field f_r by Young's modulus of elasticity E. One particular model of the residual stresses (the so-called 'polynomial model') is shown in Fig. 1(a). Under pure bending, a curvature ρ is developed at a cross-section, which induces bending strains ε_b. Making use of the usual engineering assumption that plane sections remain plane, the bending strain is defined as

$$\varepsilon_b = \rho(y - \bar{y}) \tag{1}$$

in which y is defined in Fig. 2 and $\bar{y}$ is the coordinate of the neutral axis. The strain field can be obtained simply by superposition as

$$\varepsilon = \varepsilon_b + \varepsilon_r \tag{2}$$

and the elastic-plastic-strain hardening stress-strain curve for mild steel shown in Fig. 3 allows the stress to be determined from

$$f = E\varepsilon_r + \int_{\varepsilon_r}^{\varepsilon} E_t d\varepsilon \tag{3}$$

in which E_t is the tangent modulus (either E, 0, or the strain hardening modulus E_{st} that is shown in Fig. 3). The condition of axial equilibrium requires that the axial force vanishes, so that, from Eqs. (1) and (3),
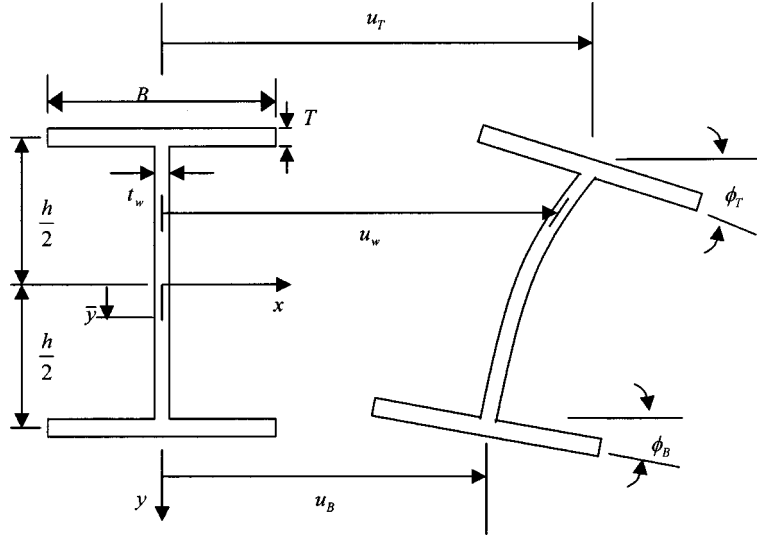
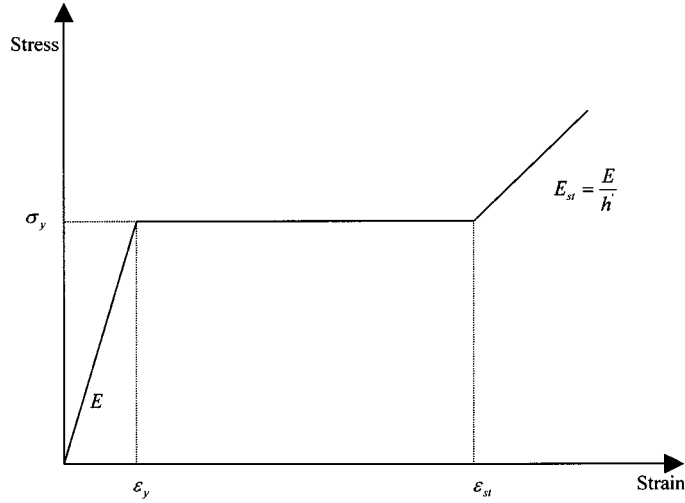Fig. 2 Deformed cross-section during buckling

Fig. 3 Constitutive modelling for mild steel

$$N \;=\; E\int_{A}\varepsilon_r dA + \int_{A}\int_{\varepsilon_r}^{\varepsilon}E_t d\varepsilon dA = \; 0 \qquad\qquad = \int_{A}\int_{\varepsilon_r}^{\varepsilon}E_t d\varepsilon dA \qquad\qquad (4)$$

which uses the axial equilibrium required for the residual stresses, in which A is the area of the cross-section. Eq. (4) may be solved at any cross-section, given a specified value of ρ in Eq. (1), to produce the neutral axis coordinate $\overline{y}$ using the technique of False Position. The appropriate tangent modulus must be used in the elastic, plastic and strain hardened regions of the cross-section, and these may be determined in the integration in Eq. (4) that is performed analytically at the cross-section level.

2.3. Out-of-plane buckling analysis

A reference buckling field M is assumed first for the cantilever (depending on the loading regime), and this is factored initially by a load factor λ. Using the M-ρ relationship developed from the in-plane analysis of the cross-section, the boundaries defining the elastic, plastic and strain hardened regions at a cross-section at a selected Gaussian station along a line element within the cantilever are determined. The constitutive relationship within each of these three regions is defined by

$$\vec{\sigma} = \overline{D}(\rho)\vec{\varepsilon} \tag{5}$$

where $\vec{\sigma}$ and $\vec{\varepsilon}$ are the generalised infinitesimal buckling stresses and strains, and $\overline{D}$ is the property matrix that depends on the curvature ρ (and so on the load factor λ) at the cross-section. The property matrix is given in Lee and Bradford (2002), and is based on a combination of orthotropic plate theory and a flow-theory based quasi-elastic modelling that does not allow for a finite unloading from the yield surface, defined simply using the von Mises criterion under uniaxial stress. The member stiffness matrix $\overline{k}(\lambda)$ can be determined using Eq. (5) together with a suitable strain matrix that is determined from lengthwise cubic interpolation polynomials (Lee and Bradford 2002). In determining this matrix, seven-point Gaussian quadrature is used along the length of the line element. The member stiffness matrix also contains the strain energy stored during buckling when the element is subjected to a dimensionless elastic translational restraint of magnitude k_t, dimensionless elastic minor axis rotational restraint of magnitude k_{ry} and dimensionless elastic twist rotational restraint of magnitude k_z that may be applied at either the top (T) or bottom (B) flange levels, respectively. These restraints are shown in Fig. 4, together with the restraining actions that they generate being applied at the flange levels.

In a similar fashion, the geometric stiffness (or stability) matrix $\overline{s}$ can be developed from a prior knowledge of the in-plane stresses f in Eq. (3). Again, seven-point Gaussian quadrature is used to determine $\overline{s}$, and the choice of the lengthwise polynomials (Lee and Bradford 2002) produces stiffness and stability matrices that are of order 16, and which are banded. The element stiffness and stability matrices may be assembled using familiar assembly techniques based on equilibrium and compatibility into their global counterparts $\overline{K}$ and $\overline{G}$ respectively.

(a) elastic restraints

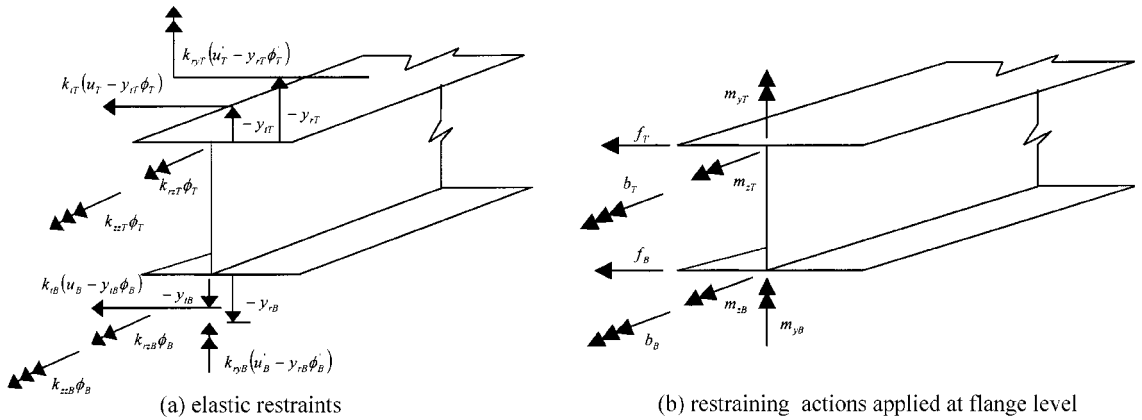(b) restraining actions applied at flange level

Fig. 4 Elastic restraints and actions

To undertake the buckling analysis, the load factor λ is increased in a proportional loading scheme, and the solution of the buckling problem can be expedited in some cases by doing this heuristically. At the given value of λ, the matrix

$$\bar{A}(\lambda) \;=\; \bar{K}(\lambda) - \bar{G}(\lambda) \tag{6}$$

is inspected. Using the technique reported in Smith *et al.* (1999), the matrix $\bar{A}(\lambda)$ is reduced to upper triangular form by Gaussian elimination without row interchanges. The determinant $|\bar{A}(\lambda)|$ is then calculated by multiplying the diagonals of the reduced matrix, and of course the value of $\lambda = \lambda_{cr}$ that makes this determinant vanish is sought. This is done by noting that the number n of eigenvalues $\lambda_{cr}^{(n)}$ less than the trial loading level λ is equal to the number of negative diagonals in the reduced $\bar{A}(\lambda)$ matrix. Once the two loading levels that bracket the first (fundamental) eigenvalue have been found, the method of bisections is used to converge upon the buckling solution to a predetermined tolerance in λ.

2.4. Verification

The numerical method has been firstly compared with the predictions of the elastic lateral-distortional buckling of cantilevers reported by Bradford (1998). The cross-sectional geometry adopted was $b_f = 200$ mm, $t_f = 20$ mm, $h = 1500$ mm and $t_w = 10$ mm, residual stresses were not included, and the yield stress f_y was set to be very large to simulate elastic behaviour. Fig. 5 shows the comparison between the elastic buckling solutions obtained from the current method using six equal-length elements, and that of Bradford (1998) who also used six elements, for a cantilever of length 15 m. The elastic restraints were non-dimensionalised as

$$\alpha_{t(T,B)} \;=\; \frac{k_{t(T,B)}L^2}{\pi^2 N_y} \tag{7}$$

$$\alpha_{ry(T,B)} \;=\; \frac{k_{ry(T,B)}}{N_y} \tag{8}$$

where $N_y = \pi^2 EI_y/L^2$ is the Euler load. In Fig. 5, the tip buckling load W_d has been non-dimensionalised with respect to the value W_{od} that is obtained without considering the effect of the elastic restraint. The comparison is very close, with discrepancies of less than 0.3% being achieved.

Since theoretical results for the inelastic distortional buckling of cantilevers appear not to have reported hitherto, and because comparisons with experiments on members should incorporate the effects of major axis curvature that are not included in the present model (Attard and Bradford 1990), the method herein was used here to demonstrate the convergence of the inelastic buckling load of an Australian 200UB25.4 cross-section (BHP 1998) with $E = 200$ GPa, v (Poisson's ratio) $= 0.3$, $f_y = 250$ MPa, $\varepsilon_{st} = 11\varepsilon_y$ and $h' = E/E_{st} = 33$. The length of the cantilever was 1952 mm. Table 1 illustrates the convergence of the inelastic buckling solution compared with that for 20 uniform elements, and it can be seen that the use of 10 uniform elements produces an error of less than 1.3% relative to the solution with 20 elements for inelastic buckling. Ten uniform elements were used in the numerical studies reported in the following section.
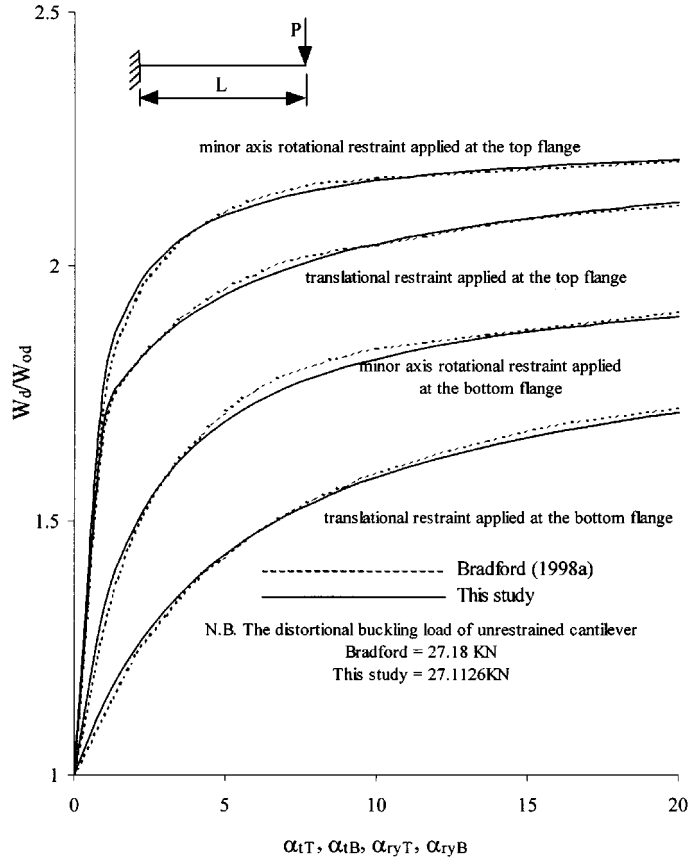
Fig. 5 Comparison with Bradford's solution

Table 1 Convergence of finite element results

Number of elements (1)	Tip buckling load (kN) (2)	Percentage difference (3)
2	26.51255	7.3
4	27.38565	4.2
6	27.78603	2.8
8	28.06204	1.9
10	28.22642	1.3
12	28.33035	0.92
14	28.4167	0.62
16	28.48605	0.37
18	28.55185	0.14
20	28.59278	-

3. Inelastic lateral-distortional buckling of cantilevers

The numerical method has been used to investigate the inelastic lateral-distortional buckling of cantilevers. Two cross-sections were used (an Australian 610UB125 with $b_f = 229$ mm, $t_f = 19.6$ mm,

Idealised diaphragm restraint: Infinite axial and
minor axis rotational restraint (membrane
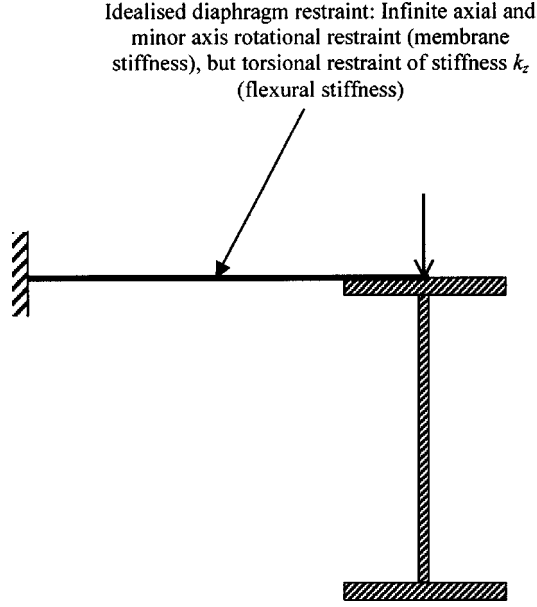stiffness), but torsional restraint of stiffness k_z
(flexural stiffness)

Fig. 6 Torsional restraint

$h = 592.4$ mm and $t_w = 11.9$ mm and an Australian 200UC46.2 with $b_f = 203$ mm, $t_f = 11.0$ mm, $h = 192$ mm and $t_w = 7.3$ mm), and these were assumed to be restrained fully against translation and minor axis rotation at the level of the top flange, but were assumed to be restrained elastically against twist rotation at the level of the top flange. An idealisation of this common restraint configuration is depicted in Fig. 6, with the dimensionless torsional restraint α_z being defined by

$$\alpha_z = \frac{k_z}{(GJ/L)} \tag{9}$$

in which k_z is the magnitude of the elastic twist restraint stiffness (which equals $3EI_r/L_r$ in Fig. 6, where I_r and L_r are the second moment of area and length of the restraint), and GJ is the Saint Venant torsional rigidity. The material properties adopted in the previous section where used for the analysis.

Commonly, residual stresses induced during the hot-rolling of universal shapes are described by two generic types, that are dependent on the manufacturing process. In Europe and Australia, the so-called polynomial model shown in Fig. 1(a) is most often used, and a prescriptive representation of this model has been given by Bradford and Trahair (1985). On the other hand, shapes rolled in North America are often described by the so-called simplified pattern of residual stress shown in Fig. 1(b), and prescriptive equations for this are well-known (Lee and Bradford 2002).

Static equilibrium of an unloaded member requires that the axial force should vanish, that the major axis bending moment should vanish, and that the minor axis bending moment should vanish. The prescriptive representations of both of these models satisfy these fundamental conditions of equilibrium. In modelling buckling, a 'Wagner' stress resultant given by
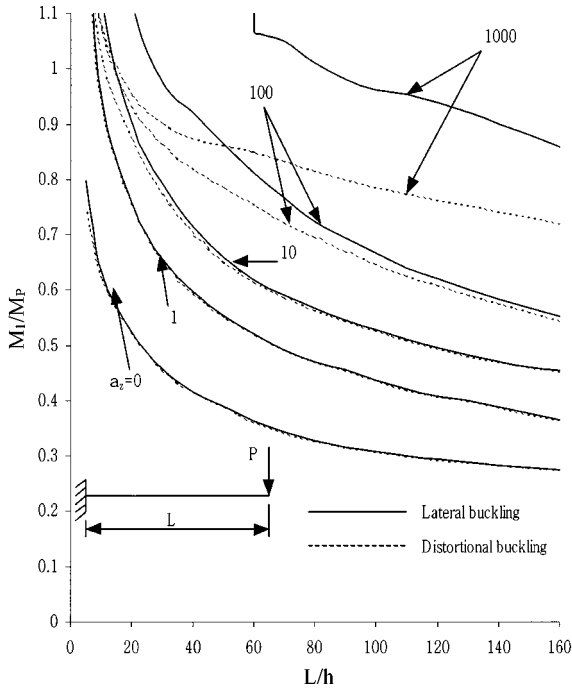
$$W = \int_A f(x^2 + y^2) dA \tag{10}$$

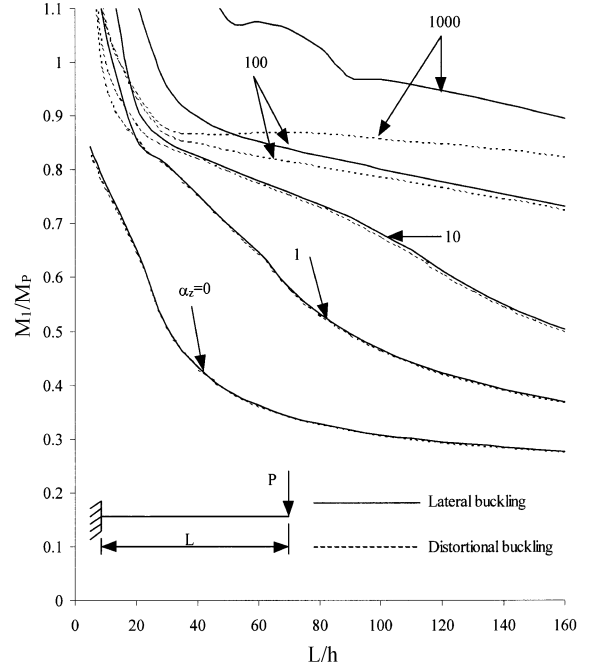Fig. 7 610UB125 with a concentrated load at the top flange (polynomial residual stresses)

Fig. 8 610UB125 with a concentrated load at the top flange (simplified residual stresses)

is encountered, and so that the inelastic and elastic solutions will coincide when the combined effects of the residual stresses and bending stresses are below yield, the Wagner parameter W should vanish. This condition is enforced in the description of the polynomial residual stress pattern given by Bradford and Trahair (1985), but not with the usual simplified residual stress patterns (Lee and Bradford 2002). So as to ensure that $W = 0$ for the simplified pattern, the tangent torsional rigidity $(GJ)_t$ that is encountered in the present finite element modelling must be reduced to $(GJ)_t - W$ in the numerical modelling. The rationale and procedure for this modification are described elsewhere (Lee and Bradford 2002).

The results for the inelastic lateral-distortional buckling of the (compact) 610UB125 with a concentrated tip load at the level of the top flange are given in Figs. 7 and 8 with the polynomial and simplified residual stress representations respectively, while Figs. 9 and 10 show the counterpart buckling results for the 610UB125 with a uniformly distributed load at the level of the top flange. In these figures, the inelastic distortional buckling moment M_I has been non-dimensionalised with respect to the plastic moment of resistance M_P of the cross-section, while the length L has been non-dimensionalised with respect to the web depth h. When $\alpha_z = 0$, the cantilever buckles about an enforced axis at the level of the top flange in a lateral-torsional mode without distortion, but as α_z increases the buckling mode displays increasing cross-sectional distortion, and indeed when $\alpha_z = 1000$ the top flange of the cantilever does not experience buckling deformations, and the buckling deformations of the bottom flange are accompanied by profound distortion of the web of the cross-section.

Figs. 11 and 12 show the respective counterpart plots of Figs. 7 and 10 respectively, but for the (non-compact) 200UC46.2 cross-section. For the deep (UB) section, it can be seen that the distortional
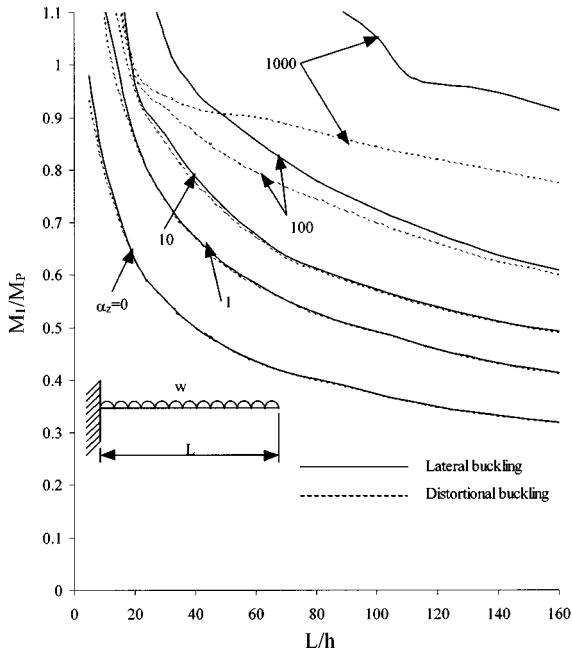
Fig. 9 610UB125 with a uniformly distributed load at the top flange (polynomial residual stresses)
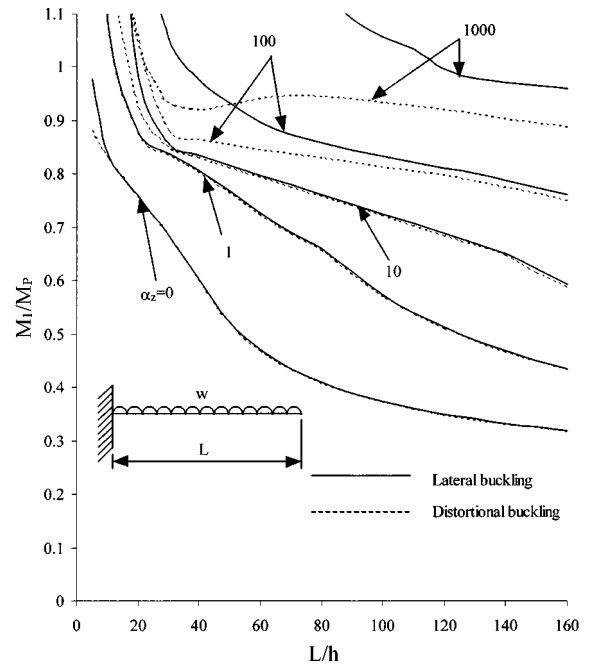
Fig. 10 610UB125 with a uniformly distributed load at the top flange (simplified residual stresses)
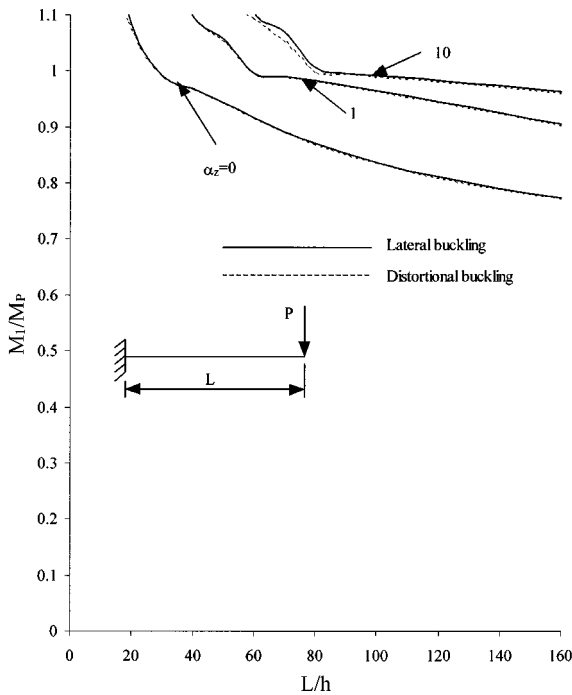
Fig. 11 210UC46 with a concentrated load at the top flange (polynomial residual stresses)
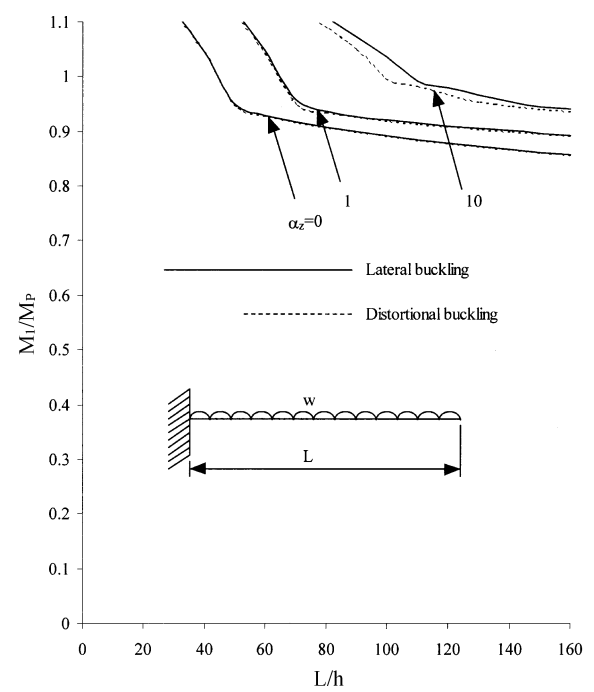
Fig. 12 210UC46 with a uniformly distributed load at the top flange (simplified residual stresses)

buckling solutions (shown dotted in Figs. 7 to 10) drop below the corresponding lateral buckling solutions as α_z increases, as the cross-sectional distortion during buckling becomes more profound. For practical beams (say $L/h < 20$), a value of $\alpha_z = 100$ is sufficient to ensure that failure will occur by the formation of a plastic hinge at M_P (and the buckling enters the strain hardening range since $M_I > M_P$) rather than by inelastic distortional buckling (when M_I is considerably less than M_P) if the beam is not laterally restrained.

A similar trend can be observed in Figs. 11 and 12 for the non-compact UC profile. However, for this beam, the non-dimensionalised buckling loads are much higher, and buckling occurs in the strain hardening range for practical beams (say $L/h < 20$), and so these beams will fail by the formation of a plastic hinge.

Finally, Figs. 7 to 12 allow for a comparison of the relative effects of the two patterns of residual stresses. It can be seen that while there is a quantifiable discrepancy between the buckling solutions using both patterns over the range of α_z, this difference can be considered as being negligible in practice.

4. Conclusions

This paper has used a finite element method of analysis, developed elsewhere by the authors, to investigate the inelastic distortional buckling of cantilevers. The method, which is described briefly, is superior to other finite element packages that require discretisation into a large number of elements, and which are unable to handle the two patterns of residual stresses (the polynomial and simplified patterns) that were considered in this study. The so-called simplified pattern must be modified so as to enforce a torsional equilibrium by the incorporation of a 'Wagner' stress resultant. The method was shown to be both efficient numerically, and accurate, by comparisons with independent studies.

Restraining the top (tension) critical flange is common in applications using I-section cantilevers. When the top flange is restrained fully against translation and minor axis rotation during buckling, but elastically against twist (as may occur with a roof sheeting that is very stiff in its membrane action, but flexible in its bending action), the restraint has a profound effect on the inelastic distortional buckling of the cantilever. This buckling is accompanied by increasing cross-sectional distortion as the torsional restraint applied at the top flange level increases, and for the two I-section profiles considered (a universal beam section and a universal column section), the restraint may inhibit overall buckling entirely for practical beam lengths, so that failure occurs due to the formation of a plastic hinge.

While the patterns of residual stresses depend on the mode of manufacture, the two common models (the polynomial pattern and the simplified pattern), although quite different in their magnitude and in their distributions across the cross-section, were shown to produce within the scope of practical design the same buckling solutions for unrestrained cantilevers and for elastically restrained cantilevers. Because of this, it can be concluded that the influence of the different types of residual stresses may be ignored in practice.

Acknowledgements

References

Anderson, J.M. and Trahair, N.S. (1972), "Stability of monosymmetric beams and cantilevers", *Journal of the Structural Division*, ASCE, **98**(ST1), 269-286.

Assadi, M. and Roeder, C.W. (1985), "Stability of continuously restrained cantilevers", *Journal of Engineering Mechanics*, ASCE, **111**(2), 1450-1456.

Attard, M.M. (1984), "The elastic flexural-torsional response of thin-walled open beams", PhD Thesis, The University of New South Wales, Sydney, NSW, Australia.

Attard, M.M. and Bradford, M.A. (1990), "Bifurcation experiments on monosymmetric cantilevers", *Twelfth Australasian Conf. on the Mechanics of Structures and Materials*, Brisbane, Australia, 207-213.

Bradford, M.A. (1988), "Buckling of elastically restrained beams with web distortions", *Thin-Walled Structures*, **6**, 287-307.

Bradford, M.A. (1990), "Distortional buckling strength of elastically restrained monosymmetric I-beams", *Thin-Walled Structures*, **9**, 339-350.

Bradford, M.A. (1992), "Buckling of doubly-symmetric cantilevers with thin webs", *Engineering Structures*, **14**(5), 327-334.

Bradford, M.A. (1998), "Distortional buckling of elastically restrained cantilevers", *Journal of Constructional Steel Research*, **14**(1-2), 3-18.

Bradford, M.A. (1999), "Elastic distortional buckling of tee-section cantilevers", *Thin-Walled Structures*, **33**(1), 3-17.

Bradford, M.A. and Trahair, N.S. (1985), "Inelastic buckling of beam-columns with unequal end moments", *Journal of Constructional Steel Research*, **5**, 195-212.

Broken Hill Proprietary Ltd. (1998), *BHP Hot Rolled Products*, BHP, Melbourne, Australia.

Lee, D.S. and Bradford, M.A. (2002), "Inelastic buckling of simply supported beams by the finite element method", submitted for publication.

Nethercot, D.A. (1973), "The solution of inelastic lateral stability problems by the finite element method", *Proceedings of 4th Australasian Conference on the Mechanics of Structures and Materials*, Brisbane, Qld., Australia, 183.

Ronagh, H.R. and Bradford, M.A. (1994), "Some notes on finite element buckling formulations for beams", *Computers and Structures*, **52**(6), 1119-1126.

Ronagh, H.R., Golestani-Rad, M. and Bradford, M.A. (2000), "Finite element instability analysis of composite bridge girders", *Proceedings of International Conference on Computational Techniques in Engineering*, Leuven, Belgium, 195-200.

Smith, S.T., Bradford, M.A. and Oehlers, D.J. (1999), "Local buckling of side-plated reinforced concrete beams. I: Theoretical study", *Journal of Structural Engineering*, ASCE, **125**(6), 622-634.

Trahair, N.S. (1993). *Flexural-Torsional Buckling of Structures*. E&FN Spon, London.

Wang, C.M. and Kitipornchai, S. (1986), "On the stability of monosymmetric cantilevers", *Engineering Structures*, **8**, 169-180.

S L